Full 2-port Vector-corrected Network Analyzer in the Acoustic Domain *

MARCUS MACDONELL, *AES Student Member* **AND JONATHAN SCOTT,** *AES Member*
(coraxaudiolabs@gmail.com) (scottj@waikato.ac.nz)

University of Waikato, Hamilton New Zealand
Corax Audio Labs, Cambridge, New Zealand

This manuscript presents the theory and design of a Vector-corrected Network Analyzer (VNA) realized in the acoustic domain. This is a novel measurement instrument based on the established microwave vector network analyzer. It employs directional couplers to separate forward and reverse traveling waves in acoustic waveguide. This instrument is intended to supersede the acoustic impedance tube. Advantages include greatly increased measurement speed and potential for traceability to external standards. Traceability is achieved by means of a calibration through an analytical solution of the error matrix produced from the measurement of a limited number of available acoustic standards. Operation is verified through analysis of the acoustic S-parameters of a passive, asymmetrical, reciprocal acoustic device constructed inside the acoustic waveguide. To the best of our knowledge this Acoustic Vector-corrected Network Analyzer (AVNA) is the first of its kind.

0 INTRODUCTION

An impedance-tube instrument like Brüel and Kjær "Standing Wave Apparatus Type 4002" was first introduced in 1955; the 4002 is still widely used today [1]. An impedance tube is typically used to measure the acoustic reflection and transmission coefficients of materials. Other methods of measuring these parameters have been reported (see for example [2, 3, 4, 5, 6]) but industry has settled on a set of standards based on the impedance tube [7, 8, 2]. These methods have no external traceability, meaning there is no physical standard, only a methodology.

An acoustic vector network analyzer (AVNA) is a device for measuring traveling waves, much like an impedance tube, but it has speed and accuracy advantages over the impedance tube [9, 10, 11]. An AVNA is capable of swept measurements at ≈200 points per minute. It offers the potential for traceability to a set of physical standards. [12] This relative speed and point density represents a huge step up in acoustic measurement. Our prototype AVNA is made using the receiver system from an HP4395A analyzer, a modified HP87511A test-set, and sets of heads based around acoustic directional couplers. Directional couplers are the key waveguide structure capable of separating forward and reverse traveling waves enabling vector network analysis. Acoustic directional couplers were first described by Lagasse [13], and used as a reflectometer by Pennington [10].

1 The Electromagnetic VNA

In the early years of Radio Frequency (RF) test and measurement there were very few techniques available to measure impedance. Such a measurement requires determining, or at least inferring, the relative or absolute magnitude and phase of the forward and reverse traveling waves present on an interconnection.

The slotted line was one of the first techniques that was developed by what is now Rohde & Schwarz. It was in world-wide commercial use by the end of the second world war. [14, 15] A slotted line permits the measurement of a Standing Wave Ratio (SWR) pattern present along a uniform transmission line. [16] The SWR pattern appears in the scalar magnitude of signal as a function of distance along the line. It is possible to infer the relative magnitudes and phases of the forward and reverse waves from the position and depth of minima in the scalloped-magnitude SWR function. [17] The slotted line is analogous to the impedance tube. The first impedance tube instrument was introduced in 1955 by Brüel and Kjær. Finding acoustic impedance using an impedance tube is still the basis of such measurements in the acoustic world today. [7, 8]

In 1965 the Wiltron 310 Vector Network Analyzer (VNA) was introduced. It was the first instrument to re-

*Correspondence should be addressed to Marcus Macdonell, coraxaudiolabs@gmail.com

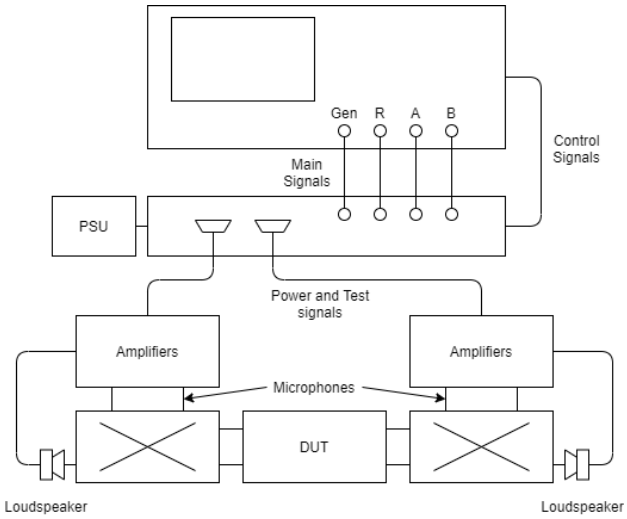

Fig. 1. Block diagram of the acoustic vector network analyzer, including power supply and modified test set, external microphone and loudspeaker amplifiers and directional couplers in the heads. The couplers are marked with the "X" crossover symbol common in microwave parlance. Shown with a device under test (DUT).

semble modern VNAs. [18] Soon after, in 1969, Hewlett-Packard brought out the model 8410A. Neither of these instruments had inbuilt vector calibration to automatically correct for errors; rather they offered the RF & microwave equivalent of the same calibration procedures employed with acoustic impedance tubes and slotted lines.

Nevertheless, both instruments were commercially successful for several reasons. There were large savings of time and effort owing to the increased speed arising from the use of directional couplers instead of slotted lines, eliminating moving parts and dispensing with any mechanical adjustment during measurement. The frequency of measurement could thus be swept automatically, and a continuous trace viewed in real time on a screen if desired. Both machines offered two ports, so that both impedance (in the form of reflection coefficient) and gain (in the form of transmission coefficient) in forward and reverse configuration (to accomodate asymmetrical devices) could be measured without complicated reconnection of the device under test (DUT). Finally, directional couplers proved to be cheaper to manufacture, since slotted lines required precision parts. [19]

All VNAs possess the same basic hardware architecture. It is the same architecture that we use in the AVNA, depicted in Figure 1, except that the electromagnetic version requires no microphones or loudspeakers to transduce between acoustic and electrical signals. The two coupled ports from each directional coupler are fed into amplifiers and then into circuits that measure the amplitude and relative phase of the four signals. These signals are usually termed a_1^M for the measured wave incident on port 1, b_1^M for the measured wave reflected from port 1, and so on. These four complex measurements are then manipulated to display whatever parameter the user desires, for example measured reflection coefficient at port 1 is

$$\Gamma_1^M = \frac{b_1^M}{a_1^M} \tag{1}$$

Calibration to remove magnitude and phase errors was achieved by placing a known short circuit in place of the DUT, and applying a fixed correction factor to gain and phase to read the known result.

The first generation of vector correction was developed in the following few years. By 1960 signal flow graphs were routinely applied to analysis of circuits composed of transmission-line interconnects. [20] Early in the 1970s, a number of researchers realised that these might be applied to VNAs. [21, 22, 23, 24] Although potentially tedious, the equations required to return the corrected parameters given the measured ones and a series of "error terms" could be found by pure algebra or through application of simple geometric rules that anyone could follow [25], although the arithmetic is sufficiently involved that it is all but impractical without a computer. The technique represented a significant theoretical advance for the VNA. By the 1980s the capacity to perform the complicated, frequency-by-frequency correction of errors was built into instruments and performed with relative ease. [18] The Hewlett-Packard 8510A "Vector-corrected Network Analyzer" incorporated the computing capability and came to dominate the industry for over a decade.

The difficult part of implementing a fully-corrected instrument lies in finding the error terms. This requires measurement of some known standards and solution of a system of equations through matrix algebra. Even in the electromagnetic domain, there are very few objects whose true impedance or transmission characteristics can be determined independently. For example, a single-port calibration to find the error coefficients demands measurement of three known, different loads, which can be especially demanding in the acoustic domain. [10]

Readers interested in the mathematical approach and solution flow can find an initial tutorial in the appendix of reference [10].

New calibration procedures, especially ones that require less knowledge about the standards, have been appearing over many years, leading to simpler and cheaper calibration methods in various general and special circumstances, see for example [26, 27, 28, 29, 30]. An excellent summary is given in [31]. A major contribution of this manuscript is the development of a calibration procedure that overcomes the difficulties enumerated in [10], enabled by the presence of two, rather than only one port.

Our prototype AVNA hardware is built around an old HP4395A Vector Network Analyzer. This instrument was designed with a separate "test set", which is to say that the parts of the instrument that involve RF, or in this case audio, components are in a separate enclosure. This arrangement is common in waveguide-based VNA designs. Thus only the test set changes in moving to the acoustic domain. Use of an existing receiver-mainframe also means that we

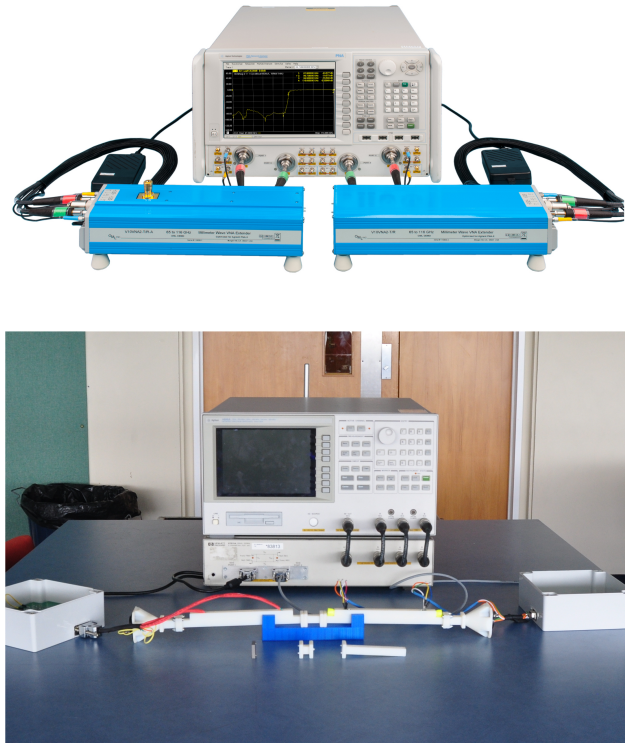

Fig. 2. A visual comparison of an Agilent (now Keysight) Technologies' Performance Network Analyzer (PNA) in the electromagnetic domain (top) and the Acoustic Vector Network Analyzer (AVNA) built for this research, fitted with 10–20 kHz heads (lower photo).

have not had to construct the phase-measurement circuits, analog-to-digital circuits, and data communications system.

2 HARDWARE

The instrument consists of two separate boxes, a so-called "test set" that contains high-frequency components including directional couplers, and a so-called "receiver" that provides data acquisition, control of the test set, signal generation from a few Hz to hundreds of megahertz, data processing, displays, and computer connectivity. We have replaced the HP87511A test set with a test set modified for acoustic, rather than electromagnetic, operation. This new test set attaches by umbilical cables to "heads" that carry the ports to which the device under test (DUT) can be connected, after the fashion of millimeter-wave and waveguide-port electromagnetic VNAs, see Figure 2. The test set will be described in more detail below. The block diagram of the measurement system is shown in Figure 1. The prototype version with low-frequency heads is shown in Figure 3.

The HP4395A instrument does not intrinsically support any waveguide or wafer calibration methods [32]. Given the receiver maximum operating frequency of 500MHz, the designers would not have anticipated a waveguide application, or that the conventional radio-frequency (RF) "Short, Open, Load, Thru" (SOLT) calibration might not be possible. Here it is used simply for data acquisition and control. The acoustic calibration methods are quite different as will be described in section 3, so these limitations are not important. The wavelengths of sound in air between a few hundred Hertz and 50kHz are the same as those of electromagnetic waves running up to almost 50GHz, as the speed of sound is a little more than one-millionth of the speed of light, so the similarity with microwave and millimeter-wave instruments is not surprising.

2.1 DIRECTIONAL COUPLERS

A Directional Coupler is a 4-port network conducting travelling waves. Figure 4 shows a symbolic directional coupler. Forward travelling waves are conducted, typically with small loss, from the input or first port P1, to the transmitted or second port, P2. Reverse travelling waves behave similarly moving from P2 to P1. Portions of the forward and reverse traveling waves are separately coupled to the two side ports. [33] It is often assumed that a directional coupler is inherently an electromagnetic device, since the majority of commercial examples have either coaxial or electromagnetic waveguide ports. In this work the directional couplers are acoustic.

The coupled port, P3, receives a portion (typically in the order of 1 %) of the forward wave power which arrives at the input port, P1, and substantially exits the transmitted port, P2. The isolated port receives the same portion of the reverse wave power that travels the other way, into P2 and out of P1. Ideally, none of the forward power appears at the isolated port, P4. The directionality of a directional coupler is a measure of the isolation between the coupled and isolated ports, i.e., how much unwanted forward power arrives at the isolated reverse side port and vice versa. Directional couplers are all imperfect; if 1% of the forward power is desirably diverted to the coupled port, one tenth or one-hundredth as much will reach the isolated port. The coupling and isolation typically both vary with frequency. Calibrations are used to measure and remove the error introduced by the directional coupler. Although the calculations can be arduous, modern computers make this practicable. Nevertheless, calibration demands some minimum directionality in order to work correctly. We believe the full two-port calibration presented in this manuscript is the first such calibration in the acoustic domain, and successfully corrects for all losses and imperfections in the directional couplers and all other hardware in the instrument.

The AVNA instrument uses a design of directional couplers presented by Lagasse in 1971. [13] The Lagasse coupler is built using a synthesis method for microwave waveguide [34] with experiment to determine the general form of a branch-line acoustic directional coupler. The key part of the structure can be seen in Figure 5, and a photograph of an example constructed in transparent acrylic in Figure 6. It may also be possible to make out the structure in Figure 3. The reader may imagine sound waves traversing from left to right above the "blocks" shown

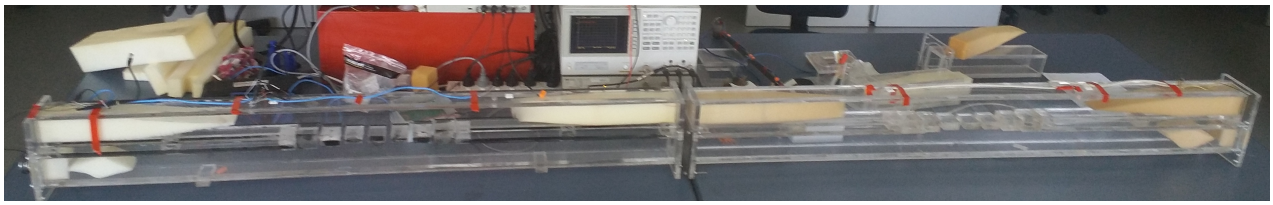

Fig. 3. The AVNA prototype setup with the much larger 1000–2000 Hz heads constructed in transparent acryllic. A DUT would be inserted between the two couplers, at bench level, where the two tables meet. Steel flange screws are just visible in the image.

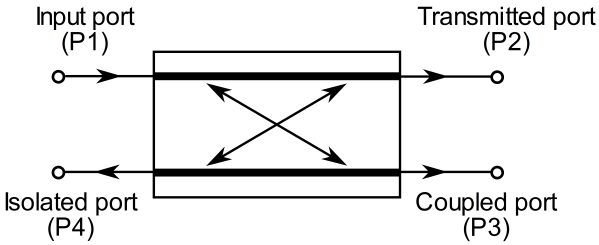

Fig. 4. A symbolic representation of a Directional Coupler with labeled ports. In spite of the naming of ports, a coupler is typically symmetrical so that it could be flipped around vertical or horizontal axes.

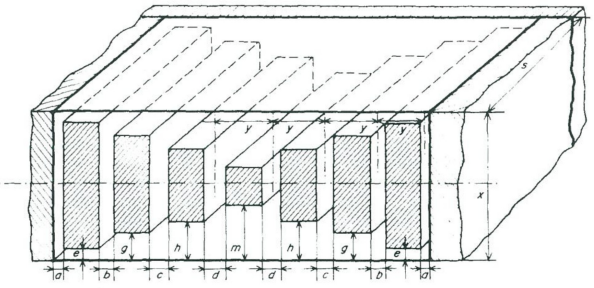

Fig. 5. The general form of the acoustic branch-line directional coupler as described by Lagasse, image taken from [13]. The reader must imagine the spaces above and below the array of gaps to be waveguides traversing left and right to form the four ports of the coupler.

in the figure. Gaps between the blocks periodically permit sound to travel downwards from the waveguide above the array of blocks to the waveguide below the array of blocks. The gaps between the blocks are the branch lines, with the width of the gaps and their spacing selected so that waves in the guide below the string of blocks interfere constructively and destructively moving left and right in the guide. This is similar to the radio frequency Butterworth and Chebyshev synthesised couplers that use the same method [34].

A version of the Lagasse design was built by Pennington and used in an acoustic impedance meter [10]. Pennington's coupler used a 60 mm square waveguide with a designed frequency range of 1–2 kHz and a usable range of 800–2,200 Hz. It had a crude flange connection system. In this work we include a 3D-printed set of couplers scaled up a decade in frequency, and improved flanges.

Fig. 6. A Lagasse coupler constructed in transparent acrylic with black tape marking the divide between parallel waveguides and the branch-line section.

2.1.1 COUPLER FLANGES AND REPEATABILITY

The directional couplers need to be connected to both the rest of the analyzer and to the DUT to function as part of the analyzer. Connections in electronics at low frequency are often paid little attention, but at high frequency and in waveguide systems in particular these connections are critical to the repeatability, precision and reliability of equipment. Microwave waveguide is typically machined from brass for reasons of precision. It usually features a rectangular cross-section and similar mounting flanges for each port. There are a number of standards for microwave flange construction and testing [35, 36]. A mechanical drawing for a commercially available WR-22 waveguide flange can be seen in Figure 7.

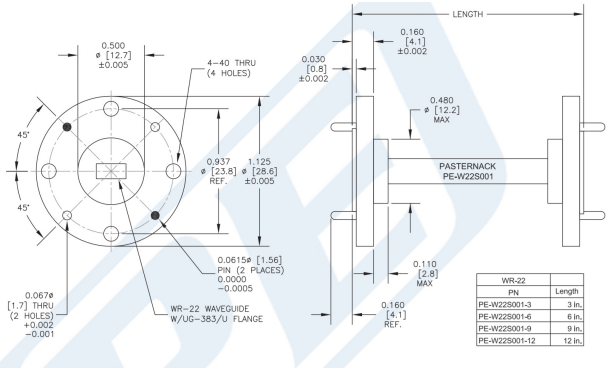

Fig. 7. WR-22 mechanical specifications taken from the datasheet for a pasternack PE-W22S001-12.

Microwave waveguide is sometimes pressurized to stop the ingress of dust and moisture. When the waveguide needs to seal O-rings can feature in microwave waveguide flange [37]. Another feature of microwave waveguide is the use of alignment pins that allow for precision mating of two flanges. Most flanges feature a bolt pattern with specific torque requirements for proper connection [38, 39, 40, 41, 42].

By borrowing from these standard microwave waveguide features, improved flanges for the acoustic coupler were developed in consultation with our university workshop. The O-ring feature was adapted to the acoustic waveguide because it is important that the waveguide seals to prevent signal leakage. The addition of alignment pins increases the ease of assembly, ensures minimum discontinuity at the junctions, and reduces sliding of the waveguide sections past one another during assembly that may scratch the mating surfaces. Figures 8 and 9 show the final designs for acoustic couplers for two bandwidths. The smaller size couplers operate over 10–20 kHz, have a guide dimension of 6 mm by 6 mm and the larger set over 1–2 kHz with the same dimensions used by Pennington.

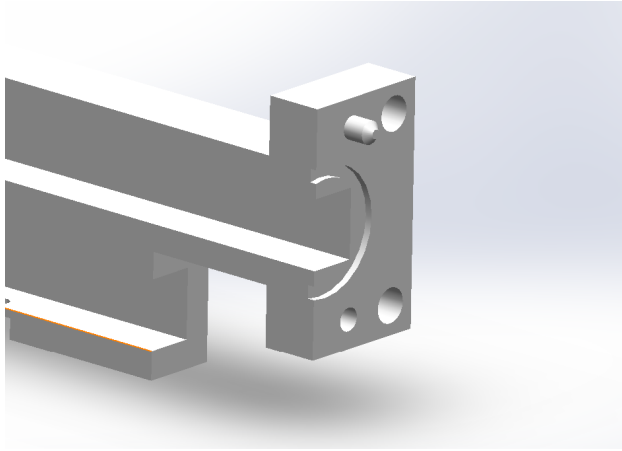

Fig. 8. A cross-section of the flange designed for the scaled and 3D printed directional couplers. This flange features an O-ring groove and alignment pins.

The performance of the acoustic waveguide flanges has been carefully studied using statistical methods. [11] This is done by taking a number of measurements of the same DUT, disconnecting it in between each measurement. It is then possible to determine the standard deviation in these measurements and then use this value as an indicator of the repeatability of the joint [11]. We concluded that even the order of tightening the flange bolts affects how repeatable is a connection. Tightening in a star pattern with a torque wrench was specified.

3 CALIBRATION

Before we can discuss calibration, we should introduce S-Parameters and the error model upon which the calibration is built.

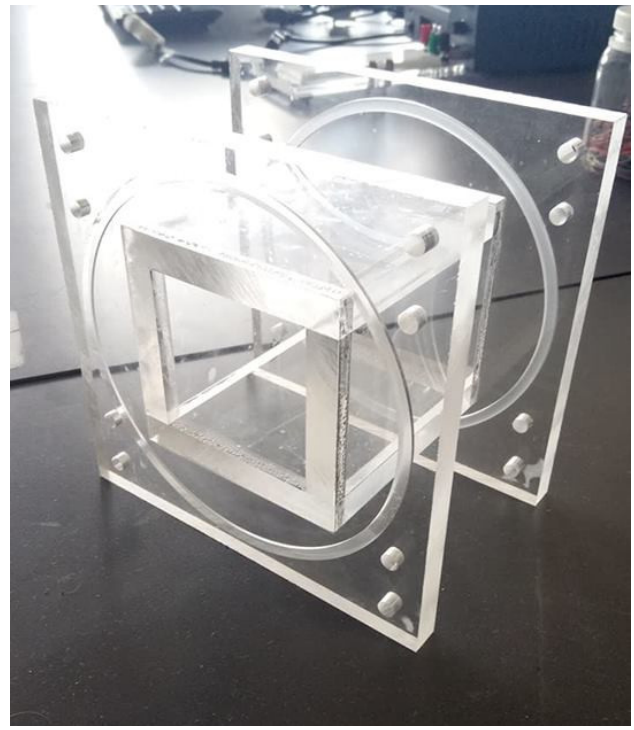

Fig. 9. An example of the larger acoustic waveguide with flanges and alignment pins visible. The component is a short length of plain waveguide, again constructed in transparent acrylic.

3.1 ACOUSTIC S-PARAMETERS

Scattering or S-parameters are used to measure the reflection and transmission coefficients of a device in the world of travelling waves, see [43] for theory and applications the RF domain, wikipedia [44] for a complete introduction & history, and [45] for a tutorial of their application in the acoustic domain. When displayed on a Smith chart, S-parameters offer an easy-to-interpret visualisation of a Device Under Test (DUT). They are routinely used in the RF world. S-parameters are equally applicable in the acoustic domain. [4, 45]

Measurement of the S-parameters for a 2-port DUT yields a set of four complex numbers. These represent of the change in signal magnitude and phase from input to output (S_{21}), output to input (S_{12}), and the input (S_{11}) and output (S_{22}) reflection coefficients. This means that the S-parameters convey impedance and gains. S_{11} is sometimes called the reflection coefficient Γ_1 for port 1, and S_{22}, Γ_2 for port 2. The complex impedance of the load is related to the reflection coefficient by the familiar formula

$$\Gamma_x = \frac{Z_x - Z_0}{Z_x + Z_0} \tag{2}$$

where Z_x is the port impedance and Z_0 is the characteristic impedance of the transmission line.

3.2 ERROR MODEL

The acoustic vector network analyzer is described with an error model that contains all sixteen terms associated with a two-port error box as has been done in the microwave domain [46, 9]. Nevertheless, it is usual in the mi-

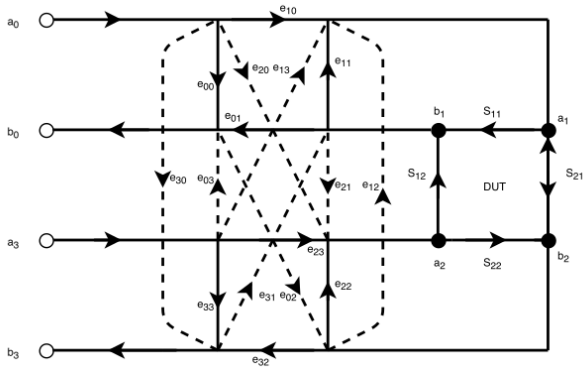

Fig. 10. A flow graph of the 16 term error model

crowave domain to truncate the 16-term model to either 12 terms in the case of planar measurements on wafer, or to 8-terms in the case of coaxial RF systems. These simplifications are possible because the physics of those situations allow a number of terms to be discarded, or more precisely to be assumed to have values that will have negligible effect. For example, one error term describes the amount of energy radiated from one port past the DUT in free space to the second port. In a coaxial system this can safely be assumed to be zero. We have observed that these simplifications lead to calibration failure in the acoustic domain. We attribute this to the imperfect guiding properties of acoustic waveguide; consider that sound energy may propagate in the walls of an acoustic waveguide, but the equivalent cannot practically occur in the electromagnetic world.

The 16-term error model can be visualized as a flow graph as shown in Figure 10 from which the equations relating measured to true S-parameters may be derived. Expressing the error model as a matrix, the equations can be solved for the unknown coefficients by means of a series of measurements for which the correct answer is known [9]. Let the error model matrix be E, then

$$E \equiv \begin{bmatrix} E_1 & E_2 \\ E_3 & E_4 \end{bmatrix} = \begin{bmatrix} e_{00} & e_{03} & e_{01} & e_{02} \\ e_{30} & e_{33} & e_{31} & e_{32} \\ e_{10} & e_{13} & e_{11} & e_{12} \\ e_{20} & e_{23} & e_{21} & e_{22} \end{bmatrix} \tag{3}$$

The relationship between the measured S-parameters S_m and the actual calibrated S-parameters S_a is by definition:

$$\begin{bmatrix} b_0 \\ b_3 \end{bmatrix} = S_m \begin{bmatrix} a_0 \\ a_3 \end{bmatrix}, \; S_m = \begin{bmatrix} S_{11m} & S_{12m} \\ S_{21m} & S_{22m} \end{bmatrix} \tag{4}$$

$$\begin{bmatrix} a_1 \\ a_2 \end{bmatrix} = S_a \begin{bmatrix} b_1 \\ b_2 \end{bmatrix}, \; S_a = \begin{bmatrix} S_{11a} & S_{12a} \\ S_{21a} & S_{22a} \end{bmatrix} \tag{5}$$

and we can then show that

$$S_m = E_1 + E_2 S_a (I - E_4 S_a)^{-1} E_3 \tag{6}$$

Where I is the unit matrix. Solving for S_a yields

$$S_a = [E_3 (S_m - E_1)^{-1} E_2 + E_4]^{-1} \tag{7}$$

Equation 7 is the result that is used to de-embed the actual S-parameters from the measured S-parameters.

In order to utilise/create a calibration method there needs to be some known standards or measurements that can be used to satisfy the equations and yield values for the error terms within the error matrix. In other words, we need to measure some devices whose S-parameters are known, in order to solve for the E matrix. In the acoustic domain we have knowledge of only a few possible standards.

- Zero length "Thru"
  A Zero length "Thru" is provided by directly coupling the two ports of the analyzer by their flanges and provides no attenuation or phase change.
- Line
  A line is less accurately known but its attenuation and phase change are related to its length. The attenuation is due to the lossy nature of air.
- Reflect
  An almost ideal reflect is provided by terminating the waveguide port with a very hard and stiff material.
- Match
  A match is provided by the sliding load method. The sliding load produces a number of points on the Smith chart; circles are then fitted to these results by the Taubin method [47, 2] and the circle center reveals the position of an ideal load. The sliding load will be discussed in detail below.

By knowing what standards we have available in the acoustic domain the number of possible methods is reduced to only a few. Most of the remaining methods are for an 8 term calibration method, which can be extended to 12 with an extra measurement. Crucially TRRM also remains, which is a method for a full 2 port 16-term calibration. The abbreviation TRRM stands for "Thru-Reflect-Reflect-Match", meaning that only a through connection of some sort, two reflection scenarios, and a match are required. [48] TRRM was selected because it is achievable with the available standards. Using TRRM in order to solve for the 16-term model, five measurements are required. A Thru, Match-Match, Reflect-Reflect, Match-Reflect and Reflect-Match. These measurements produce five sets of measured S-parameter matrices that have a corresponding known "actual" S-parameter matrix.

The ideal matrices are:

$$\text{Thru:} \quad A = \begin{bmatrix} 0 & T \\ T & 0 \end{bmatrix} \tag{8}$$

$$\text{Match-Match:} \quad B = \begin{bmatrix} 0 & 0 \\ 0 & 0 \end{bmatrix} \tag{9}$$

$$\text{Reflect-Reflect:} \quad C = \begin{bmatrix} \Gamma & 0 \\ 0 & \Gamma \end{bmatrix} \tag{10}$$

$$\text{Reflect-Match:} \quad D = \begin{bmatrix} \Gamma & 0 \\ 0 & 0 \end{bmatrix} \tag{11}$$

$$\text{Match-Reflect:} \quad E = \begin{bmatrix} 0 & 0 \\ 0 & \Gamma \end{bmatrix} \tag{12}$$

$$\tag{13}$$

T is known from the length l and propagation constant γ, where $T = e^{-\gamma l}$, for a zero length Thru, $T = 1$.

Equation 7 is very non-linear and difficult to solve directly. Cascading T-parameters can be used to linearize the problem. Solving for the T parameters can be done in a variety of ways. Two common methods are normalizing by one of the unknown coefficients and solving directly or using a least squares method. Single value decomposition (SVD) is used often because of its ability to handle singularities [49, 48].

The E and T matrices are related by the following:

$$E = \begin{bmatrix} T_2 T_4^{-1}, & T_1 - T_2 T_4^{-1} T_3 \\ T_4^{-1}, & -T_4^{-1} T_3 \end{bmatrix} \tag{14}$$

$$T = \begin{bmatrix} E_2 E_1 E_3^{-1} E_4, & E_1 E_3^{-1} \\ E_3^{-1} E_4, & E_3^{-1} \end{bmatrix} \tag{15}$$

Substituting the T matrix into the system yields:

$$\begin{bmatrix} b_0 \\ b_3 \\ a_0 \\ a_3 \end{bmatrix} = T \begin{bmatrix} a_1 \\ a_2 \\ b_1 \\ b_2 \end{bmatrix} \tag{16}$$

Using the T parameters and the definitions of S_m and S_a the following can be derived

$$S_m = (T_1 S_a + T_2)(T_3 S_a + T_4)^{-1} \tag{17}$$

$$T_1 S_a + T_2 - S_m T_3 S_a - S_m T_4 = 0 \tag{18}$$

$$S_a = (T_1 - S_m T_3)^{-1}(S_m T_4 - T_2) \tag{19}$$

Equation 19 is the new de-embedding equation and allows for a solution of the error model. The results of both the analytical and numerical methods are presented in this manuscript.

3.3 PHYSICAL STANDARDS

In order to utilise the calibration method there needs to be actual physical known standards that can be used to satisfy the equations and yield an error matrix. The standards required in this case are:

- Zero length "Thru"
  A Zero length "Thru" is provided by directly coupling the two ports of the analyzer by their flanges and provides no attenuation or phase change.
- Reflect
  An virtually ideal reflect is provided using a 5 mm mild steel plate to close the guide.
- Match
  A match is provided by the sliding load method where the load is a foam wedge free to move within a length of open waveguide. In this work we used 5 points per frequency, suitably selected [50, 51]. Circles were then fitted to these results by the Taubin method [47, 2] and the circle center taken as the result that would have been measured had an ideal load been used.

Commercial vector network analyzers often have an optional (often expensive) calibration kit such as the one pictured in Figure 11. These production standards must be produced with very high precision and tolerances so that any customer can be confident that their results are reproducible in other laboratories around the world.

Fig. 11. An Agilent 85056A 2.4 mm VNA calibration kit including sliding loads and calibration data.

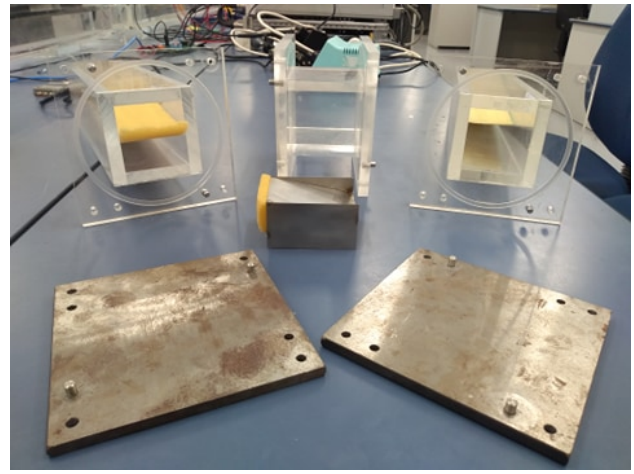

Fig. 12. A full set of acoustic standards. Large Reflect standards made from 5 mm mild steel plate, front left and right. Large Match standards made from open cell foam in a section waveguide, rear left and right. In the middle is a finite-lenghth "thru", in front of which is an inclusion after the fashion of that to be described around Figure 14.

A full set of standards that make up the 1-2 kHz acoustic calibration kit can be seen in Figure 12. A Line, or "Thru" of non-zero length was also built, since it is of known length it is possible to know the phase change through its length for each frequency making it a potential acoustic standard. The zero-length Thru is achieved by connecting both ports together repeatably by using a specific bolt pattern and bolt torque [11]. The "Reflect" is achieved by closing off the port with a 5 mm mild steel plate, us-

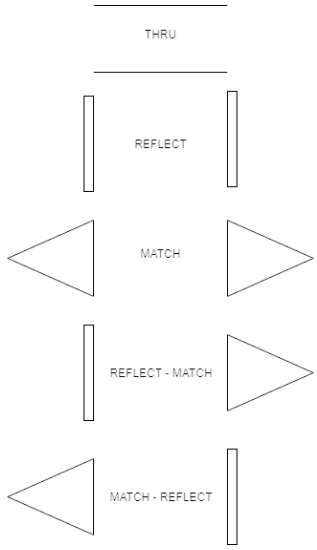

Fig. 13. A symbolic representation of the standards as connected to the analyzer for each of the five total measurements. The left hand column is the port one standards in order, port two is the right hand column

ing the same bolt pattern and torque. The idea is that a sufficiently-massive end-plate completely reflects incident sound. The Match (a load with negligible reflecion) is provided by a section of waveguide that contains a wedge section of foam, again using the same bolt pattern and torque. This section of foam is used as an acoustic analogue of the "Sliding load" that was used in radio-frequency (RF) VNA calibrations and Pennington's acoustic impedance meter. [50, 10].

The standards are connected in order and their four S-parameters are measured. The sliding loads for each of the "Match" measurements are slid to several positions and measured as discussed in some detail in section 3.3.1. The standards are represented symbolically in Figure 13. The figure shows the connections required for each of five measurements. The standards in order that are connected to port one are shown in the left hand column while those that are connected to port two are on the right.

3.3.1 THE SLIDING LOAD

A sliding load is used to separate the magnitude of any residual reflection due to the imperfections of a practical load. The magnitude of any fixed reflection from the actual load is assumed not to change with position of the absorber. The reflection from the load can be separated from other reflections in the system by sliding the load and using the resulting phase change. In the electromagnetic case, magnitude of the reflection from the load does not change with position, but the phase does. In the acoustic case the change in length means that the reflection magnitude may be reduced with increased distance from the source. This means in the acoustic case any lossy line or waveguide will result in a spiral locus on a Smith chart [10]. We discovered in practice the loss is often small enough that the spiral may be assumed to be a circle, as in the electromagnetic case.

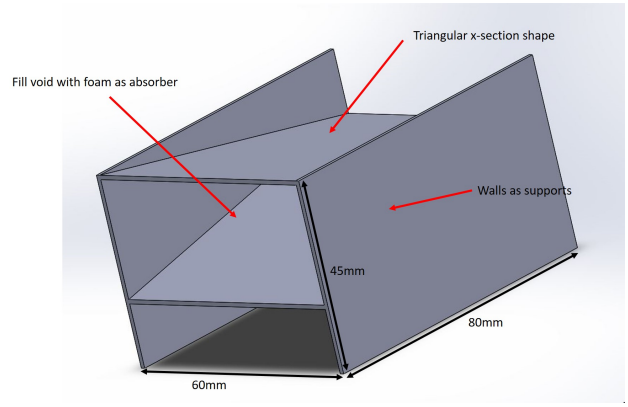

Fig. 14. A 3D CAD model for the Asymmetrical element to be inserted into a section of waveguide, creating the Asymmetrical "Thru"/transmission line verification standard. This CAD model can be 3D printed to implement the Asymmetrical element.

The circle or spiral fit is realised with a numerical method. On occasion that method can return unsatisfactory results, most commonly when the combination of frequency and load positions leads to measurements clustered rather than distributed alround the circle. These points are readily detected in the processing phase and can be automatically removed.

4 VERIFICATION

4.1 ASYMMETRICAL TRANSMISSION LINE STRUCTURE

An asymmetrical, reciprocal device embedded in a transmission line has the following characteristics: $S_{12} = S_{21}$ and $S_{11} \neq S_{22}$ [52]. If such an asymmetrical device's orientation is reversed and it is then measured again, swapped-around S-parameters S'_{11}, S'_{12}, S'_{21}, and S'_{22} are obtained. Then if $S'_{11} = S_{22}$, $S'_{22} = S_{11}$, $S'_{12} = S_{21}$, and $S'_{21} = S_{12}$ the calibration has successfully accounted for the error adapters on both ports.

An asymmetrical device was made by folding some light gauge steel sheet into a 'V' shape and filling the space between with foam. Sides were added that extend past the 'V' so that it can be placed in the waveguide and rest on the bottom surface. This structure, when placed in a length of waveguide will provide the characteristics of an asymmetrical transmission line. Figure 14 shows the 3D model for the device, and Figure 15 shows the physical implementation. This device was constructed to fit a 60 mm by 60 mm waveguide, and inserted in a short length of suitable guide.

The asymmetrical transmission line was measured in two orientations, forward and reverse. In the forward orientation, the nose of the triangular structure is pointed towards port one, and in the reverse orientation pointed towards port two. The forward and reverse response of S_{11} & S_{21} for the asymmetrical transmission line is shown in Figure 16. This response has typical transmission values of close to 0 dB while the magnitude of the reflection tends to increase with frequency from typical values below 40 dB to below 20 dB.

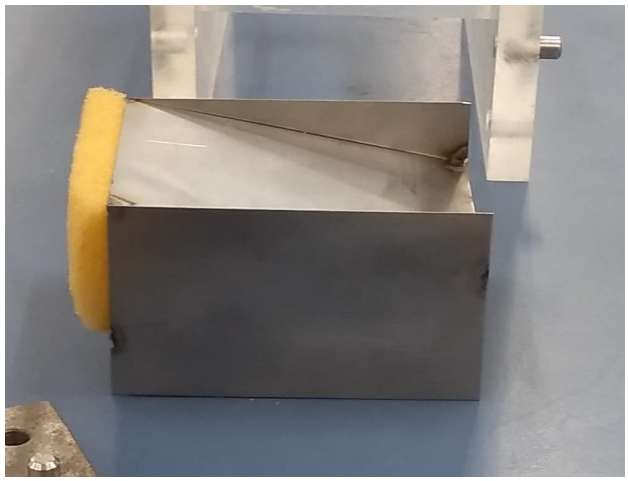

Fig. 15. The Asymmetrical element made from thin steel sheet (0.9 mm) and a foam wedge, this structure is then placed in a section of waveguide to complete the vitrifaction standard.

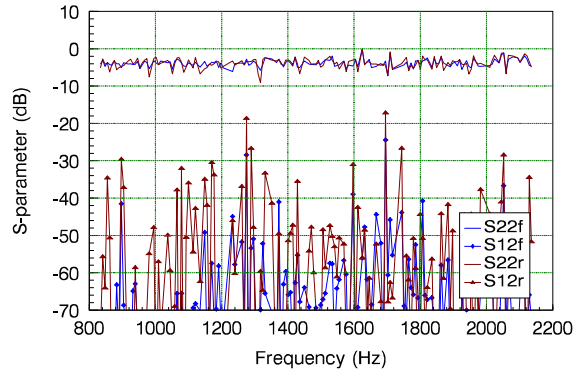

Fig. 17. Comparison of S_{22} and S_{12} measured on the asymmetrical element inserted each way around. Again the legend has S'_{22} as S_{22r}, etc. The parameters measured in the forward orientation, S_{12f} and S_{22f} agree strongly with the parameters measured in the reverse orientation S_{12r} and S_{22r}.

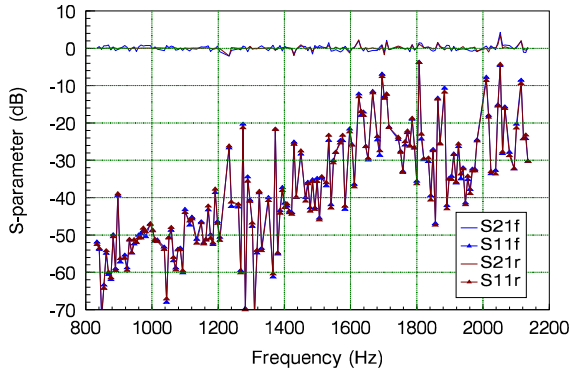

Fig. 16. Comparison of S_{11} and S_{21} measured on the asymmetrical element inserted each way around. In the legend, S_{21} is labelled S_{21f} and S'_{21} is labelled S_{21r}, etc. Note that S_{21} measured in the first case is virtually indistinguishable from S'_{21} measured with the device physically inserted the other way around. Likewise the input side reflection coefficient S_{11} differs by only small values despite its enormous variability.

The reverse response mirrors the forward orientation and has typical transmission values of close to 0 dB while the magnitude of the reflection tends to increase with frequency from typical values below 40 dB to below 20 dB.

The forward and reverse response of S_{22} & S_{12} for the asymmetrical transmission line is shown in Figure 17. This response has typical transmission values of -4 dB while the magnitude of the reflection tends to be small.

The repeatability of measurements using the acoustic network analyzer has been shown to have a worst case standard deviation of 0.4 dB [11]. The difference between the forward and reverse orientations for S_{11}, S'_{22}, S_{21}, and S'_{12} is less than 1 dB in most cases. The standard deviation for $S_{11} - S'_{22}$ is 0.506 dB and 0.694 dB for $S_{21} - S'_{12}$. The reflection coefficient is small, and we attribute the increased variance to random noise [9, 11]. The variance is consistent with the repeatability of the instrument suggesting that the calibration is performing well.

4.2 Comparison of Calibration Computation Methods

The same results should be expected when using either the analytical or numerical solutions to the error matrix. Figures 18 and 19 show the calibrated results using both methods. These results agree strongly for the transmission coefficients S_{21} and S_{12} and less strongly for the reflection coefficients S_{11} and S_{22}. The numerical method on average returns slightly greater reflection coefficients and with greater variance, the transmission coefficients follow very closely with a slight increase in variance as well. The variation in the reflection coefficients can be attributed to the variation in measurements used for the numerical method that are excluded from the analytical one. This is because the five calibration measurements produce an overdetermined system. In order to calibrate analytically, duplicate information is not used whereas in the numerical method it is left in leading to a slight increase in variance.

The numerical measurements of the asymmetrical transmission line also show that the calibration has been successful. The forward and reverse measurements agree, with a slight increase in variance compared to the analytical method. There is a small variation increase for the results calibrated with the numerical solution of the error matrix.

Because the results of the analytical and numerical calibration are in a agreement and consistent with what would be expected of an asymmetrical, reciprocal device [52] we are confident that the AVNA is now complete and validated. Further validation can be achieved with comparison to results simulated by means of CFD, but this is beyond the scope of the present work. It should also be noted that there are no physical standards that exist to allow for

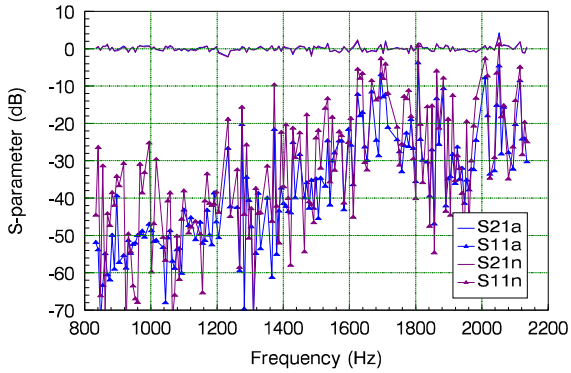

Fig. 18. Comparison of parameters S_{21} and S_{11} obtained by numerical and analytic solution of the error matrix. The same raw measurements of standards are used in each case.

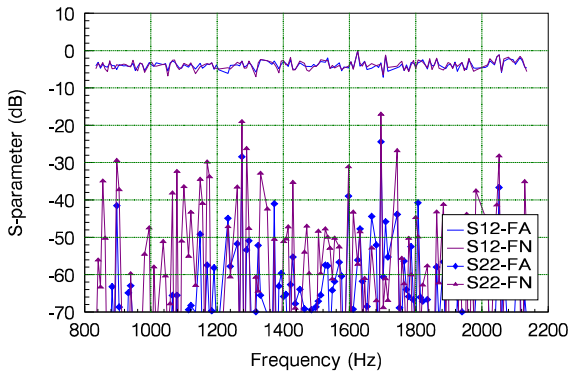

Fig. 19. Comparison of parameters S_{12} and S_{22} obtained by numerical and analytic solution of the error matrix. The same raw measurements of standards are used in each case.

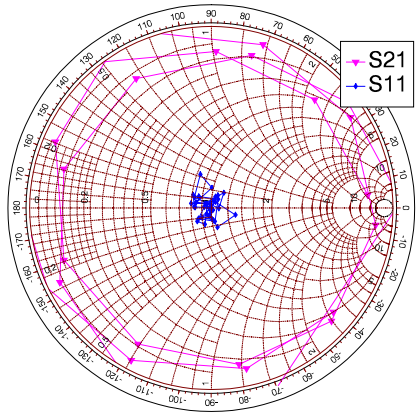

Fig. 20. The S_{11} and S_{21} values of an uncorrected thru connection plotted on a Smith chart. Frequency runs from 1220 Hz to 1980 Hz.

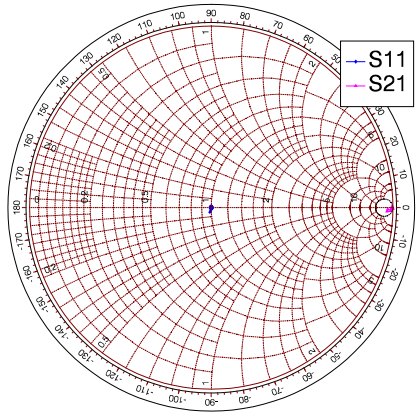

Fig. 21. The S_{11} and S_{21} values of a zero-length thru after correction plotted on a Smith chart. The zero-length thru data are close to being points so appear as single symbols.

the comparison of this measurement instrument to another. Alas, this is one of the problems the authors wish to address with the development of the AVNA.

4.3 Comparison of Corrected and Uncorrected Data

Figures 20 and 21 present uncorrected and corrected measurements of a zero-length thru re-connection. The data is presented in Smith Chart form, as is customary in the RF world. Smith charts present magnitude and phase, but sacrifice the visibility of frequency. Data runs from 1220 to 1980 Hz. The plots are presented separately as the corrected data for a zero-length thru appears as a single point and can be hard to identify. The uncorrected data shows the wildly-varying magnitude and phase typical of raw data. In the case of Figure 21, the zero-length thru data is indicative of the repeatability error. Some data has been removed, especially between 1780 and 1820 Hz, owing to low confidence caused by the selection of sliding load positions. On our prototype it is not possible to check coverage gaps resulting from load position selections in real time, as might be the case on an integrated real-time instrument.

5 SUMMARY AND CONCLUSIONS

This manuscript presents the first acoustic, vector-corrected, 2-port, network analyzer. Like any new high-performance measurement instrument, there are several separate advances required to realise the final instrument. There must be hardware that achieves directionality, for which we have relied upon a decades-old design by Lagasse, elegant but neglected. There must be calibration and verification standards. For these, we have mined the rich history of electromagnetic VNAs, adapting technologies such as the sliding load and (passive) asymmetric, reciprocal devices to the acoustic domain. There must be an

interconnection mechanism for the acoustic waveguides that is highly repeatable, for which we designed a flanged system with inbuilt O-ring seals, 3D-printed in titanium in the case of higher frequencies and smaller parts. Finally and most importantly, a series of measurements of known standards must be devised that permits solution for all the error coefficients in the system. This manuscript presents a pathway to find the 16 complex error coefficients of a general 2-port travelling-wave system that correct out the imperfections of the couplers and measurement electronics. This is the calibration procedure. We investigated both an analytical and a numerical approach to solving the error matrix, identifying the performance differences between these two approaches. We have shown that the AVNA instrument achieves its aim of measurement of acoustic reflectivity and transmissivity.

A notable advance of this work lies in the standards required for calibration. All previous acoustic measurement systems have relied to some extent upon calibration against a standard that is not well known. For example, [4] assumed a load, and [10] relied upon lossy lines. Here only an uncertain load and a reflection plate are required.

This manuscript reports the culmination of several years of work. Following in the footsteps of early electromagnetic vector network analyzer development, we have successfully built a prototype instrument capable of fast, swept, acoustic measurements. We have verified its operation. We have demonstrated operation in two frequency bands; extension to cover the audio spectrum is now possible. We consider that this represents a compression of some 5-plus decades of radio-frequency measurement experience into the acoustic domain.

One criticism of this design is that each set of heads spans just over an octave. Covering a reasonable audio spectrum would require 8 to 10 test sets. This same criticism was directed at EM VNAs as they moved from a few GHz bandwidth, past 100 GHz to the present terahertz range, each waveguide step adding less than one octave of bandwidth. As time passed, directional sensing structures with ever-increasing bandwidth were developed, and multiple couplers were incorporated into single head structures. By the end of the last century couplers whose highest operational frequency was 1000 times their lowest operational frequency became available. We believe the same will occur when sufficient need appears in the acoustic domain. An advantage of the acoustic impedance tube is that it can be made to span the human audio range. [6] With fixed-position microphones, the method relies upon a numerical fit to separate the forward and reverse waves. Each scheme has its advantages and disadvantages.

Applications of this instrument will continue to be found in the future. For now we suggest

- rapid, precise measurement of the reflectivity of architectural and furnishing materials,
- measurement of the sound transmissivity of building insulation materials and seals,
- determination of the resonant properties of cabinets, tubes, and cavities such as speaker enclosures and engine exhaust structures,
- characterisation of musical instrument components such as organ and brass pipes,
- energy absorption provided by cavity filling materials,
- sonar visibility of insects and other small items,
- impact on sonar visibility of surface coatings,
- indirect measurement of biological properties of flora correlated with sound absorption and reflection,
- non-destructive testing of composite structures, and
- plastic weld inspection.

Finally, we see no reason that a test set could not be constructed with water in place of air as the conducting medium. This would allow testing in an aquatic sonar scenario.

6 ACKNOWLEDGMENT

This research was partially funded by the "science for technological innovation" (SfTI) science challenge, one of the New Zealand national science challenges. (http://www.sftichallenge.govt.nz/) The authors wish to acknowledge the assistance of Peter Higgins in the Waikato University workshop.

7 REFERENCES

[1] "Technical review 1955-1 standing wave apparatus_1955," Tech. rep., Bruel and Kjaer (1955 Jan).

[2] K. Pennington, *Acoustic Vector Network Analyser*, Ph.D. thesis, The University of Waikato, Hamilton, New Zealand. (2017).

[3] J. Smith, C. Fritz, J. Wolfe, "A new technique for the rapid measurement of the acoustic impedance of wind instruments," *Proc. Seventh International Congress on Sound and Vibration* (2000 July).

[4] C. M. De Blok, R. F. M. Van den Brink, "Direct-Reading One-Port Acoustic Network Analyzer," *Journal of The Audio Engineering Society*, vol. 41, no. 4, pp. 231–238 (1993 April).

[5] J. Price, "Acoustic VNA User's Guide," (2008 January), URL `https://spot.colorado.edu/~pricej/downloads/AVNAUsersGuide.pdf`.

[6] R. Schlieper, S. Li, J. Peissig, "Development and validation of a full audio range acoustic impedance tube," presented at the *144th Convention of the AES, Milan, Italy*, pp. 1–4 (2018 May).

[7] "Acoustics – Determination of sound absorption coefficient and impedance in impedance tubes – Part 1: Method using standing wave ratio," Standard, International Organization for Standardization, ISO Central Secretariat, Chemin de Blandonnet 8, CP 401 - 1214 Vernier, Geneva, Switzerland (1996).

[8] "Acoustics – Determination of sound absorption coefficient and impedance in impedance tubes – Part 2: Transfer-function method," Standard, International Organization for Standardization, ISO Central Secretariat,

Chemin de Blandonnet 8, CP 401 - 1214 Vernier, Geneva, Switzerland (1996).

[9] M. MacDonell, J. Scott, "Realizing an Acoustic Vector Network Analyzer," *Proc. 147th Audio Engineering Society Convention* (2019).

[10] J. Scott, K. E. Pennington, "Acoustic Vector-Corrected Impedance Meter," *IEEE Transactions on Instrumentation and Measurement*, vol. 63, no. 12, pp. 2726–2732 (2014), [Online]. Available: 10.1109/TIM.2014.2327474.

[11] M. MacDonell, K. Basnet, J. Scott, "Waveguide Joint Design and Validation for use in Acoustic Vector-corrected Network Analysers," presented at the *2019 IEEE International Instrumentation and Measurement Technology Conference (I2MTC)*, pp. 1–5 (2019), [Online]. Available: 10.1109/I2MTC.2019.8826926.

[12] K. Wong, "Traceability of vector network analyzer measurements," doi:10.1109/ARFTG.2008.4804283, pp. 157–167 (2008).

[13] P. Lagasse, "The realization of an acoustical directional coupler," *Journal of Sound and Vibration*, vol. 15, no. 3, pp. 367 – 372 (1971), [Online]. Available: https://doi.org/10.1016/0022-460X(71)90430-5.

[14] F. E. Terman, *Radio Engineering* (McGraw-Hill Book Co.), 3rd ed. (1947).

[15] W. B. Wholey, "Greater Reliability in UHF Impedance Measurements," *HP Journal Vol. 1*, vol. 53, no. 5 (1950), URL `http://www.hparchive.com/`.

[16] M. Golio, *The RF and Microwave Handbook* (CRC Press) (2001).

[17] S. Y. Liao, *Microwave Devices and Circuits* (Prentice-Hall), 3rd ed. (1990).

[18] D. Rytting, "ARFTG 50 year network analyzer history," presented at the *2008 71st ARFTG Microwave Measurement Conference*, pp. 1–8 (2008), [Online]. Available: 10.1109/ARFTG.2008.4633319.

[19] "Slotted Line," *Wikipedia* (retrieved March 2021), URL `https://en.wikipedia.org/wiki/Slotted_line`.

[20] Mason, Zimmerman, *Electronic Circuits, Signals & Systems* (Wiley) (1960).

[21] S. Rehnmark, "On the Calibration Process of Automatic Network Analyzer Systems," *IEEE Transactions on Microwave Theory and Techniques*, vol. 22, pp. 457–458 (1974).

[22] B. P. Hand, "Developing accuracy specifications for automatic network analyzer systems," *Hewlett-Packard Journal*, pp. 16–19 (1970 February).

[23] W. Kruppa, K. Sodomsly, "An explicit solution for the scattering parameters of a linear two-port measured with an imperfect test set," *IEEE Transactions on Microwave Theory and Techniques*, vol. 19, pp. 122–123 (1971 January).

[24] H. V. Shurmer, "Calibration procedure for computer-corrected parameter characterisation of devices mounted in microstrip," *Electronics Letters*, pp. 323–324 (1973 July).

[25] Kuhn, "Signal Flow Graphs," *Microwave Journal*, p. 59 (1963 November).

[26] G. Engen, C. Hoer, "Thru-reflect-line: An improved technique for calibrating the dual six-port automatic network analyzer," *IEEE Trans. Microwave Theory Tech.*, vol. 27, no. 12, pp. 987–993 (1979).

[27] K. J. A. Davidson, E. Strid, "LRM and LRRM calibrations with automatic determination of load inductance," *36th ARFTG Conference digest*, pp. 57–63 (1990).

[28] A. Ferrero, U. Pisani, "Two-Port Network Analyzer Calibration Using an Unknown Thru," *IEEE Microwave and Guided Wave Letters*, vol. 2, no. 12, pp. 505–507 (1992 December).

[29] L. Hayden, "An Enhanced Line-Reflect-Reflect-Match Calibration," *Proceedings of the 67th IEEE ARFTG Conference*, pp. 143–149 (2006).

[30] C. Huang, H. Lin, "A Novel Calibration Algorithm With Unknown Line-Series-Shunt Standards for Broadband S-Parameter Measurements," *IEEE TRANSACTIONS ON INSTRUMENTATION AND MEASUREMENT*, vol. 57, no. 5 (2008 may).

[31] A. Rumiantsev, N. Ridler, "VNA Calibration," *IEEE Microwave Magazine*, pp. 86–99 (2008 June).

[32] Agilent, "Agilent 4395A Network/ Spectrum/ Impedance Analyzer Operation Manual," (2007 May), URL `https://literature.cdn.keysight.com/litweb/pdf/04395-90040.pdf`.

[33] P. Rizzi, *Microwave Engineering - Passive Circuits* (Prentice-Hall Inc, Englewood Cliffs NJ) (1988).

[34] R. Levy, L. F. Lind, "Synthesis of Symmetrical Branch-Guide Directional Couplers," *IEEE Transactions on Microwave Theory Techniques*, vol. 19, no. 2, pp. 80–89 (1968 feb), [Online]. Available: 10.1109/TMTT.1968.1126612.

[35] "Flanges for waveguides - Part 1: General requirements," Standard, International Electrotechnical Commission, Geneva (2016).

[36] "Flanges for waveguides - Part 2: Relevant specifications for flanges for ordinary rectangular waveguides," Standard, International Electrotechnical Commission, Geneva (2016).

[37] "Sealing test for pressurized waveguide tubing and assemblies," Standard, International Electrotechnical Commission, Geneva (2016).

[38] T. N. Anderson, "Rectangular and Ridge Waveguide," *IRE Transactions on Microwave Theory and Techniques*, vol. 4, no. 4, pp. 201–209 (1956), [Online]. Available: 10.1109/TMTT.1956.1125063.

[39] M. Horibe, K. Noda, "Modification of waveguide flange design for millimeter and submillimeter-wave measurements," *77th ARFTG Microwave Measurement Conference*, pp. 1–7 (2011).

[40] M. Horibe, R. Kishikawa, "Performance of new design of waveguide flange for measurements at frequencies from 800 GHz to 1.05 THz," *79th ARFTG Microwave Measurement Conference*, pp. 1–6 (2012).

[41] M. Horibe, "Measurement Uncertainty in Terahertz VNAs: Using Terahertz Vector Network Analyzers for Stable, Accurate Measurement and to Evaluate Uncertainty," *IEEE Microwave Magazine*,

vol. 19, no. 2, pp. 24–34 (2018), [Online]. Available: 10.1109/MMM.2017.2779678.

[42] "IEEE Standard for Rectangular Metallic Waveguides and Their Interfaces for Frequencies of 110 GHz and Above–Part 2: Waveguide Interfaces," *IEEE Std 1785.2-2016*, pp. 1–22 (2016), [Online]. Available: 10.1109/IEEESTD.2016.7564020.

[43] R. E. Collin, *Foundations for Microwave Engineering* (Wiley-IEEE Press) (2001).

[44] Wikipedia, "Scattering parameters," .

[45] W. Koontz, "Multiport Acoustic Models with Applications in Audio Signal Processing," *Journal of the Audio Engineering Society*, vol. 61, no. 10, pp. 727–736 (2013 October).

[46] H. Van Hamme, M. Vanden Bossche, "Flexible vector network analyzer calibration with accuracy bounds using an 8-term or a 16-term error correction model," *IEEE Transactions on Microwave Theory and Techniques*, vol. 42, no. 6, pp. 976–987 (1994), [Online]. Available: 10.1109/22.293566.

[47] G. Taubin, "Estimation of planar curves, surfaces, and nonplanar space curves defined by implicit equations with applications to edge and range image segmentation," *IEEE Transactions on Pattern Analysis and Machine Intelligence*, vol. 13, no. 11, pp. 1115–1138 (1991).

[48] K. Silvonen, "LMR 16-a self-calibration procedure for a leaky network analyzer," *IEEE Transactions on Microwave Theory and Techniques*, vol. 45, no. 7, pp. 1041–1049 (1997).

[49] J. V. Butler, D. K. Rytting, M. F. Iskander, R. D. Pollard, M. Vanden Bossche, "16-term error model and calibration procedure for on-wafer network analysis measurements," *IEEE Transactions on Microwave Theory and Techniques*, vol. 39, no. 12, pp. 2211–2217 (1991), [Online]. Available: 10.1109/22.106567.

[50] H. C. Heyker, "The Choice of Sliding Load Positions to Improve Network Analyser Calibration," presented at the *1982 12th European Microwave Conference*, pp. 429–434 (1982), [Online]. Available: 10.1109/EUMA.1982.333099.

[51] G. Vandersteen, Y. Rolain, J. Schoukens, A. Verschueren, "An improved sliding-load calibration procedure using a semiparametric circle-fitting procedure," *IEEE Transactions on Microwave Theory and Techniques*, vol. 45, no. 7, pp. 1027–1033 (1997), [Online]. Available: 10.1109/22.598437.

[52] J. B. Scott, "Investigation of a method to improve VNA calibration in planar dispersive media through adding an asymmetrical reciprocal device," *IEEE Transactions on Microwave Theory and Techniques*, vol. 53, no. 9, pp. 3007–3013 (2005), [Online]. Available: 10.1109/TMTT.2005.854225.

THE AUTHORS

Marcus MacDonell

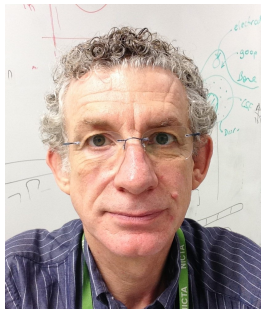

Jonathan Scott

Marcus attended The university of Waikato in Hamilton, New Zealand from 2010 to 2020, and was awarded a BE(hons) in 2014, and a Master of Engineering in 2015. Marcus founded Corax Audio labs in 2016 with seed money awarded by the Summer Start-Up Program at the University of Waikato. His PhD research marries the fields of vector network analysis and acoustic measurement.

●

Jonathan has worked as an EE for universities and private industry in Australia, California and for the last 15 years as a professor of electronics engineering at the University of Waikato in New Zealand. His research focuses on characterization, measurement, modeling and simulation, especially at RF & microwave frequencies. Recent work has strong biomedical context revolving around modeling electrodes for human implantation, and techniques for making implant leads safe in MRI scanners. Other research includes acoustic measurement, fractional-order equivalent-circuit modeling and characterization of lithium batteries, and engineering education especially in the context of threshold concepts.